The Duffing Oscillator

Student Name: Damon Binder
Student ID: u5591488
Course: PHYS3301

Contents

1. Introduction

1.1 The Duffing Oscillator

The Duffing Oscillator can be interpreted as describing a spring which does not obey Hooke's law. Unlike in simple harmonic motion, where the restoring force is linear, for the Duffing Oscillator the restoring force is given by:

$$F = -(\alpha x + \beta x^3)$$

where x is the displacement from central position, and where $\alpha < 0$ and $\beta > 0$. Thus, in the unforced and undamped case, the Duffing Oscillator can be described by the equation:

$$m\ddot{x} + \alpha x + \beta x^3 = 0$$

By adding a damping term $2\gamma\dot{x}$ and a sinusoidal driving force given $F\cos(\omega t)$, we have the full Duffing Oscillator, satisfying the equation:

$$\ddot{x} + 2\gamma\dot{x} + \alpha x + \beta x^3 = F\cos(\omega t)$$

This equation is known as the Duffing Equation. As this is a second order differential equation, in order to fully determine the equation we must know the initial position x_0 and velocity $\dot{x}_0$ of the oscillator.

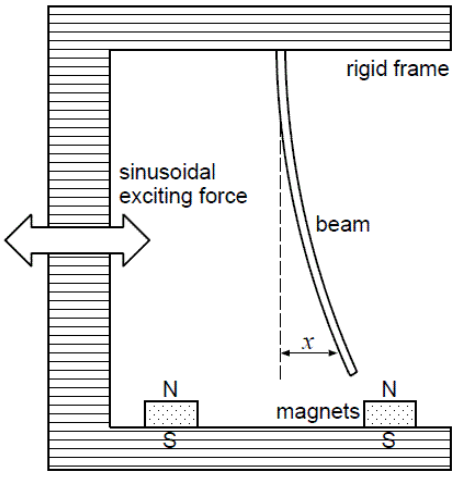

Diagram 1: Physical example of a Duffing Oscillator (Kanamaru, 2008)

This equation describes many different physical systems. One such example is a steel beam hanging from a rigid beam between two magnets. The beam can be driven by applying a sinusoidal force to the frame. This system is shown in *Diagram 1.*

Electronic analogues of the Duffing Oscillator can also be created (Tamasevicuite, Tamasevicius, Mykolaitis, Bumeliene, & Lindberg, 2008).

1.2 Dimensional Analysis

The Duffing Oscillator is described by the differential equation:

$$\ddot{x} + 2\gamma\dot{x} + \alpha x + \beta x^3 = F\cos(\omega t)$$

with initial conditions $x(0) = x_0$, $\dot{x}(0) = \dot{x}_0$, where γ and β are positive and α is negative. As the cosine function is even, we can also take ω as positive. Define:

$$y = x\frac{\sqrt{\beta}}{\omega}$$
$$\tau = \omega t$$

Then:

$$\frac{dx}{dt} = \frac{dx}{d\tau}\frac{d\tau}{dt} = \frac{\omega^2}{\sqrt{\beta}}\dot{y}$$
$$\frac{d^2x}{dt^2} = \frac{\omega^3}{\sqrt{\beta}}x_0\ddot{y}$$

where the derivative of y are taken with respect to τ. Thus, we can write the Duffing Oscillator as:

$$\frac{\omega^3}{\sqrt{\beta}}\ddot{y} + 2\gamma\frac{\omega^2}{\sqrt{\beta}}\dot{y} + \frac{\alpha\omega}{\sqrt{\beta}}y + \frac{\omega^3}{\sqrt{\beta}}y^3 = F\cos(\tau)$$

Dividing through by $\frac{\omega^3}{\sqrt{\beta}}$:

$$\ddot{y} + \frac{2\gamma}{\omega}\dot{y} + \frac{\alpha}{\omega^2}y + y^3 = \frac{F\sqrt{\beta}}{\omega^3}\cos(\tau)$$

Let:

$$a = \frac{2\gamma}{\omega}, \qquad b = -\frac{\alpha}{\omega^2}$$
$$G = \frac{F}{\omega^2 x_0}$$

We can now write the Duffing Oscillator as:

$$\ddot{y} + a\dot{y} - by + y^3 = G\cos(\tau)$$

All these parameters are unitless, and a and b are positive. The number of parameters has been reduced from seven to five.

For the remainder of the report, we shall work with the Duffing Oscillator in this form. However, for convenience, we shall switch back to using t and $x(t)$ rather than τ and $y(\tau)$. We shall now write the equation for the Duffing Oscillator as:

$$\ddot{x} + a\dot{x} - bx + x^3 = G\cos(t), \qquad x(0) = x_0, \qquad x'(0) = \dot{x}_0$$

1.3 Symmetry

So far we have reduced the Duffing equation to:

$$\ddot{x} + a\dot{x} - bx + x^3 = G\cos(t)$$

for positive a and b. We shall now show that the behaviour of the oscillator when G is negative is the same as the behaviour when G is positive. Let $x(t)$ solve the Duffing equation, and define $z(t) = x(t+\pi)$. Then:

$$\ddot{z} + a\dot{z} - bz + z^3 = \ddot{x}(t+\pi) + a\dot{x}(t+\pi) - bx(t+\pi) + \big(x(t+\pi)\big)^3$$
$$= G\cos(t+\pi) = -G\cos(t)$$

and thus:

$$\ddot{z} + a\dot{z} - bz + z^3 = -G\cos(t)$$

We can conclude that the solutions of the Duffing Oscillator for negative G are simply the solutions of the Duffing Oscillator with positive G shifted in time by half a period. For this reason, we only need to consider the behaviour of the oscillator for positive G.

This relationship also suggests a discrete symmetry possessed by the Duffing oscillator. Let $y(t) = (-1)^n x(t + n\pi)$. Then:

$$\ddot{y} + a\dot{y} - by + y^3 = (-1)^n \left(\ddot{x}(t + n\pi) + a\dot{x}(t + n\pi) - bx(t + n\pi) + \big(x(t + n\pi)\big)^3\right)$$
$$= (-1)^n G\cos(t + n\pi) = G\cos(t)$$

And therefore, if $x(t)$ solves the Duffing Oscillator, then so does $(-1)^n x(t + n\pi)$.

2. Approximations to the Duffing Oscillator

2.1 Unforced and Undamped Duffing Oscillator

When the Duffing Oscillator is both undamped and unforced, $a = G = 0$, and the Duffing equation reduces to:

$$\ddot{x} - bx + x^3 = 0, \qquad x(0) = x_0,\ x'(0) = \dot{x}_0$$

Multiplying this by $\dot{x}$ gives:

$$\dot{x}\ddot{x} - b\dot{x}x + \dot{x}x^3 = 0$$

Thus:

$$\frac{d}{dt}\left(\frac{\dot{x}^2}{2} - \frac{bx^2}{2} + \frac{x^4}{4}\right) = 0$$

Therefore, the quantity:

$$E(x, \dot{x}) = \frac{\dot{x}^2}{2} - \frac{bx^2}{2} + \frac{x^4}{4}$$

is a conserved quantity. We can interpret this as the energy of the system, with $\frac{\dot{x}^2}{2}$ being the kinetic energy and $-\frac{bx^2}{2} + \frac{x^4}{4}$ being the potential energy.

To understand the implications of this, it is useful to separate the Duffing Oscillator into two first order ODEs, by defining:

$$y = \dot{x}$$

We then have the system of equations:

$$\dot{x} = y$$
$$\dot{y} = y^2 - bx + cx^3$$

the solution of which is completely determined once an initial (x, y) value is given. While the equation itself cannot be solved analytically, we can use the fact that energy is conserved in order to find the trajectory of the system through phase space:

$$E(x, y) = \frac{y^2}{2} - \frac{bx^2}{2} + \frac{x^4}{4} = E_0$$

where E_0 is the initial energy of the system. Thus, the trajectory through phase space of the system must fall on a contour of $E(x,y)$.

To determine the shape of the contours of $E(x,y)$, we first note that

$$\lim_{x^2+y^2\to\infty} E(x,y) \to \infty$$

and thus any contour must lie within a bounded region of space. This means that any contour of $E(x,y)$ must be comprised of a finite set of isolated points and closed curves. The isolated points must be either maxima or minima of $E(x,y)$. Also, the intersection of any contour with itself must be a saddle point of $E(x,y)$ and thus, we begin by determining the critical points of $E(x,y)$:

$$\nabla E(x,y) = \mathbf{0}$$

This is equivalent to:

$$2y = 0$$
$$x^3 - bx = 0$$

Therefore, $y = 0$ and either $x = 0$ or:

$$x = \pm\sqrt{b}$$

To determine what type of critical points these represent, we must calculate the Hessian at these points:

$$H_E(x,y) = \begin{pmatrix} E_{xx} & E_{xy} \\ E_{xy} & E_{yy} \end{pmatrix} = \begin{pmatrix} 3x^2 - b & 0 \\ 0 & 1 \end{pmatrix}$$

At the origin, the Hessian is indefinite and we can conclude that the origin is a saddle point.
At $\left(\pm\sqrt{b},0\right)$, the Hessian is positive definite, and therefore these two points are the points of minimum energy. Thus, the minimum energy of the system is:

$$E\left(\sqrt{b},0\right) = E\left(-\sqrt{b},0\right) = -\frac{b^2}{2} + \frac{b^2}{4} = -\frac{b^2}{2}$$

At the origin, $E(0,0) = 0$. Therefore, the contour $E(x,y) = 0$ intersects itself at the origin. As we have found all critical points of the system, we can deduce the following:

1) The only stationary points of the system are the origin and $\left(\pm\sqrt{b},0\right)$
2) If the system has energy between $-\frac{b^2}{2}$ and 0, then it has a periodic solution, centred around either $\left(\sqrt{b},0\right)$ or $\left(-\sqrt{b},0\right)$
3) If the energy of the system is 0, then the system will limit towards the origin
4) If the energy of the system is larger than 0, then the system has a periodic solution, encompassing both $\left(\sqrt{b},0\right)$ and $\left(-\sqrt{b},0\right)$

Examples of such paths are shown in *Diagram 2*.

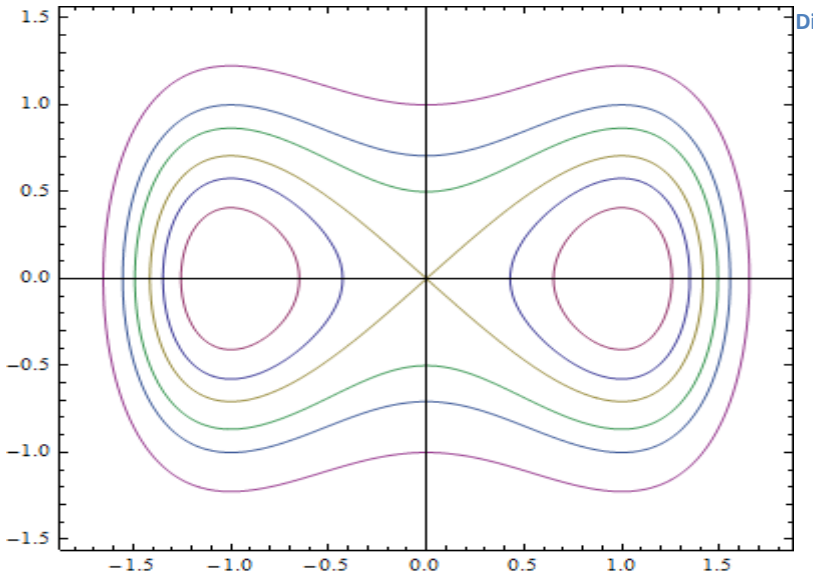

Diagram 2: Paths of constant energy for $b = 1$

2.2 Unforced Duffing Oscillator

We shall now include damping in our calculations. The Duffing equation is thus:

$$\ddot{x} + a\dot{x} - bx + x^3 = 0$$

Again, we can multiply by $\dot{x}$, and we find that:

$$\dot{x}\ddot{x} - b\dot{x}x + \dot{x}x^3 = -a\dot{x}^2$$

$$\frac{d}{dt}\left(\frac{\dot{x}^2}{2} - \frac{bx^2}{2} + \frac{x^4}{4}\right) = -a\dot{x}^2$$

Using the same definition of energy as before, we have thus deduced that:

$$\frac{dE}{dt} = -a\dot{x}^2 \leq 0$$

as both a and $\dot{x}^2$ are positive. From this equation we can deduce that any stable solution has to satisfy $\dot{x}(t) = 0$. If this is the case, then $x(t) = x_s$, and thus, in to find these we must solve:

$$-bx_s + x_s^3 = 0$$

There are three possibilities. Either $x_s = 0$, or $x_s = \pm\sqrt{b}$. These points correspond to the three critical points of the undamped system. The origin is not a stable point, and the other two points are stable stationary points. If the system starts with negative energy, then it will spiral into the closest stable stationary point. Otherwise, it will cycle around both until its energy drops to below 0, at which point it will spiral to the closest stable stationary point.

There is another possible path that the system may follow; it may limit to the origin. This can be seen by examining points that are arbitrarily close to the origin. In this case, the cubic term can be ignored, and we have the equation:

$$\ddot{x} + a\dot{x} - bx = 0$$

The general solution of this equation is:

$$x(t) = c_1 e^{t\frac{\left(-a+\sqrt{a^2+4b}\right)}{2}} + c_2 e^{t\frac{\left(-a-\sqrt{a^2+4b}\right)}{2}}$$

As $-a+\sqrt{a^2+4b} > 0 > -a-\sqrt{a^2+4b}$, we note that the first term is unstable but the second term is stable and will limit towards the origin. Thus, if we choose initial conditions such that $c_1 = 0$ then the system will limit to the origin. To achieve this, taking $t = 0$ the initial conditions must satisfy:

$$x_0 = c_2$$
$$\dot{x}_0 = c_2 \frac{-a-\sqrt{a^2+4b}}{2}$$

or more simply:

$$\frac{\dot{x}_0}{x_0} = \frac{-a-\sqrt{a^2+4b}}{2}$$

We conclude that in the case of points that are sufficiently close to the origin satisfying the above ratio, then the unforced Duffing Oscillator will limit to the origin. However, we can then take these points and use them as initial conditions to solve the time reversed equation derived from the substitution$\tau = -t$. At any point along the solution curves, the system will limit to the origin. They split the phase space into two regions, and as no solution path can cross another solution path, any point that starts in one of the two regions must remain in that region. However, all points other than those on the boundary will limit to one of the two stable points. We can conclude that there is a stable point in each region, and thus one region contains all the points limit to one stable point, while the other region contains all the points limiting to the other stationary point. An example is shown in *Diagram 3* where $a = b = 1$, created by taking $x_0 = \pm 0.01$ and $\dot{x}_0 = \mp 0.01\varphi$, and then numerically solving the time-reversed equation.

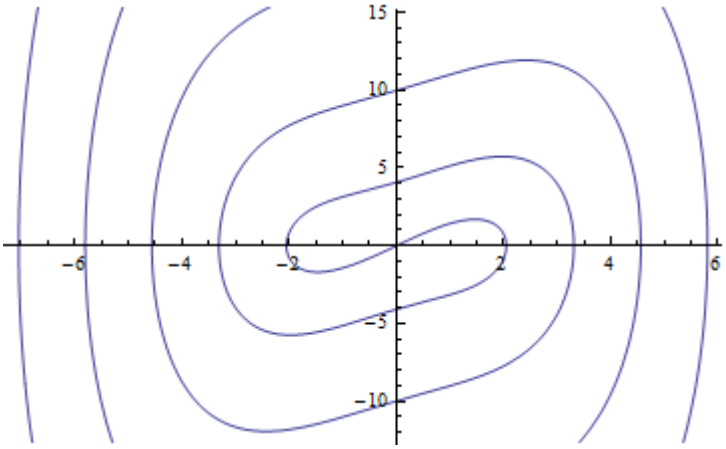

Diagram 3: Paths limiting to 0 when $a = b = 1$. If an initial condition is in the same region as (1,0) then it limits to this point, otherwise it limits to (-1,0)

2.3 A Small Driving Force

We shall now deal with the full Duffing Oscillator:

$$\ddot{x} + a\dot{x} - bx + x^3 = G\cos t\,, \qquad x(0) = x_0,\ x'(0) = \dot{x}_0$$

Again, we can multiply through by $\dot{x}$ and then integrate to get the energy. Continuing to define energy as:

$$E(x,\dot{x}) = \frac{\dot{x}^2}{2} - \frac{bx^2}{2} + \frac{x^4}{4}$$

we find that the derivative of energy is now:

$$\frac{dE}{dt} = G\dot{x}\cos t - a\dot{x}^2$$

Assume that G is far smaller than a. We can then expect that, if the system starts far from one of the minimum points, then the system will lose energy until it becomes close to either of the two points. For the rest of this analysis, we shall assume that the system is always very close to a minimum point. At the minimum points the function:

$$-bx + x^3 = 0$$

and close to these points we can approximate these terms with a linear term:

$$-bx + x^3 \approx \left(x - \sqrt{b}\right)\left(3\left(\sqrt{b}\right)^2 - b\right) = 2b\left(x - \sqrt{b}\right)$$

To simplify the analysis and make obvious the parallel between this situation and the damped and driven simple harmonic oscillator, we shall now set shift the minimum point to the origin by using the transform $x' = x - \sqrt{b}$. The new equation of motion is now:

$$\ddot{x}' + a\dot{x}' + 2bx' = G\cos t,$$

which is simply the equation for a damped and driven harmonic oscillator. We wish to find the limit cycle of this system. From the theory of linear differential equations, we know that there is a unique steady-state solution to this equation. To find the steady-state solution, we can substitute:

$$x' = m\cos t + n\sin t$$

into the equation. We find:

$$-m\cos t - n\sin t - ma\sin t + na\cos t + 2bm\cos t + 2bn\sin t = G\cos t$$

Equating the coefficients of sine and cosine:

$$G = -m - na + 2bm$$
$$0 = -n + ma + 2bn$$

Using the second equation:

$$m = n\frac{(1-2b)}{a}$$

Substituting this into the first equation:

$$G = n\left(-\frac{1-2b}{a} - a + 2b\frac{1-2b}{a}\right)$$
$$aG = n(-a^2 - 1 + 4b - 4b^2)$$

and thus:

$$n = \frac{-aG}{a^2 + (2b-1)^2}$$

$$m = \frac{G(2b-1)}{a^2 + (2b-1)^2}$$

Thus:

$$x' = \frac{G(2b-1)}{a^2 + (2b-1)^2}\cos t + \frac{-aG}{a^2 + (2b-1)^2}\sin t$$

and therefore:

$$x(t) = \frac{G(2b-1)}{a^2 + (2b-1)^2}\cos t + \frac{-aG}{a^2 + (2b-1)^2}\sin t + x_m$$

For a small driving force, we have derived an approximate formula for the two limit cycles, one around each minimum point:

$$x(t) = \frac{G(3b^2-b-1)}{a^2 + (1+b-3b^2)^2}\cos t + \frac{-aG}{a^2 + (1+b-3b^2)^2}\sin t \pm \sqrt{b}$$

In phase space the curve $\big(x(t), \dot{x}(t)\big)$ forms a circle centred around $\big(\pm\sqrt{b}, 0\big)$, and whose radius varies linearly with G. The radius can be found explicitly by substituting $t = 0$ the equation:

$$\begin{aligned} r &= \sqrt{\big(x(0) - \sqrt{b}\big)^2 + \dot{x}(0)^2} \\ &= G\sqrt{\left(\frac{2b-1}{a^2 + (2b-1)^2}\right)^2 + \left(\frac{-a}{a^2 + (2b-1)^2}\right)^2} \\ &= G\sqrt{\frac{a^2 + (2b-1)^2}{(a^2 + (2b-1)^2)^2}} \\ &= \frac{G}{\sqrt{a^2 + (2b-1)^2}} \end{aligned}$$

We can verify this numerically by calculating the radius for a large number of t values and then finding the maximum and minimum for various values of G. This is done in *Diagram 4* in the case of $a = b = G = 1$. For small values of G the maximum and minimum radii are close, and well approximated by $r = \frac{G}{\sqrt{2}}$.

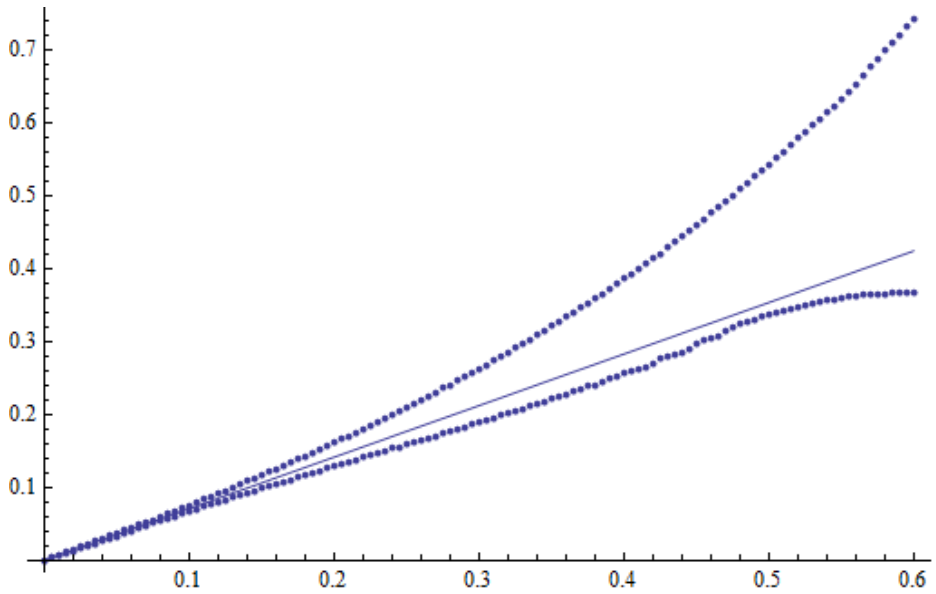

Diagram 4: Maximum and minimum radius plotted against G. The straight line is the function $r = \frac{G}{\sqrt{2}}$.

3. Chaos

3.1 Definition of Chaos

So far the approximations of the Duffing Oscillator we have studied have all demonstrated regular behaviour. However, we shall now turn our attention to regions of parameter space where the behaviour is chaotic. Choas is defined to be the occurrence of bounded aperiodic behaviour in a deterministic system with sensitive dependence on initial conditions (Kaplan & Glass, 1995). The Duffing Oscillator is a deterministic system, as the coordinate of the system at any point in time can be used to determine the evolution of the oscillator through all time. Boundedness means that the solutions always remain within a finite interval of phase space, aperiodic means that no solutions do not form limit cycles, and sensitivity to initial conditions means that points that are initially close together will diverge over time. We begin by arguing that the Duffing Oscillator is bounded.

3.2 Boundedness of Solutions

We shall study the situation where the energy of the Duffing Oscillator is very large:

$$E(x,\dot{x}) = \frac{\dot{x}^2}{2} - \frac{bx^2}{2} + \frac{x^4}{4} \gg 0$$

In this situation, at least one of $|x|$ and $|\dot{x}|$ must be large. We first assume that $|\dot{x}| \gg 0$. In this situation the change in energy:

$$\frac{dE}{dt} = G\dot{x}\cos t - a\dot{x}^2$$

will be negative, as:

$$G\dot{x}\cos t < G|\dot{x}| < a|\dot{x}|^2 = a\dot{x}^2$$

for sufficiently large values of $|\dot{x}|$. From this inequality, we can deduce that for $|\dot{x}|$ to be sufficiently large its value must be around $\frac{G}{a}$. Therefore, when $|\dot{x}| \gg 0$ the energy will decrease.

Now we shall examine the case of $|x| \gg 0$ and $\dot{x}^2 \approx 0$. In this regime the Duffing Equation can be approximated as:

$$\ddot{x} + a\dot{x} - bx + x^3 = G\cos t \Rightarrow \ddot{x} + x^3 = 0$$

The right hand differential equation describes a particle in a quartic potential, and it is evident that such a particle would oscillate in a manner analogous to the harmonic oscillator. In particular, it will start at a point of high potential energy, and it will increase in speed until it passes through the equilibrium point with a high kinetic energy. If we choose a sufficiently large initial displacement, we can make the maximum kinetic energy arbitrarily large. Therefore, if $|x|$ is made sufficiently large, the approximation we made will result in $|\dot{x}| \gg 0$, placing us in the first approximation where the energy of the system decreases. We can conclude that if the energy is sufficiently large, then the energy will decrease over time.

As the energy of the system decreases when the energy is sufficiently large, we know that there is some energy, E_0, above which the energy of the system always decreases. We can conclude that solutions to the Duffing Oscillator must be bounded.

This argument is not fully rigorous, but it could be made rigorous if more care were taken to find bounds on the error of the approximations. However, for our purposes it does provide a good heuristic explanation for the boundedness of solutions to the Duffing Oscillator.

3.3 Transition to Chaos

To study the development of chaos in the Duffing Equation, we shall examine the case of $a = 0.5$ and $b = 1$. For small values of G, there are two limiting cycles, approximated by the results in section 2.3. These cycles have period 2π. Once the driving force reaches a critical point, around 0.3427, the limit cycle becomes unstable and is replaced by a limit cycle of period 4π. This cycle then becomes unstable at around $G = 0.3549$, with the period doubling again to 8π. This process of period doubling continues, with $G = 0.3578$ creating a period of 16π, a period of 32π occurring at $G = 0.35848$, and a period of 64π being produced at $G = 0.35861$. The rate of period doubling increases as the size of the period increases, resulting in the production of arbitrarily long cycles for values of G around 0.3589. This progression of period doubling is shown in *Diagram 5.*

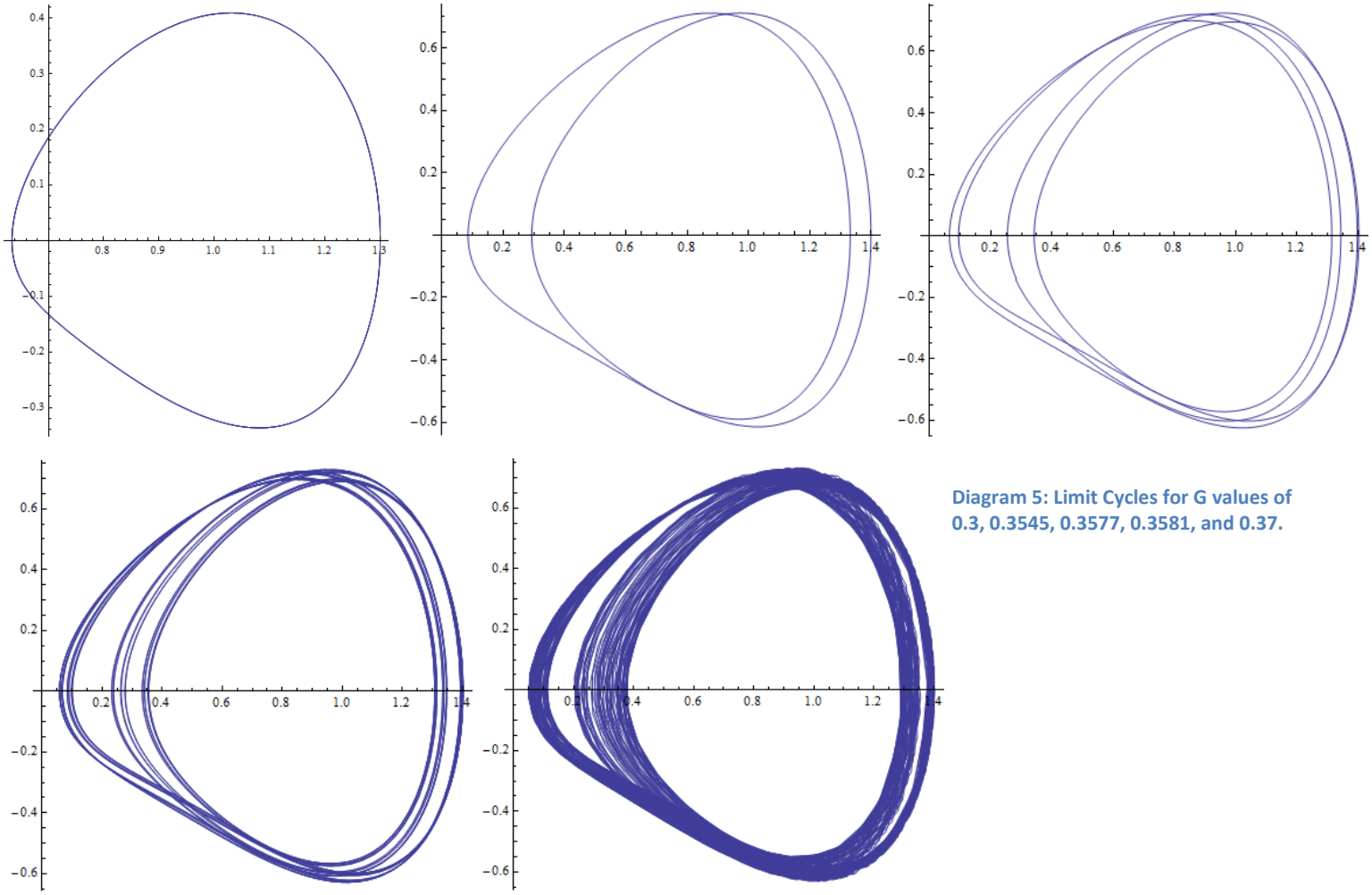

Diagram 5: Limit Cycles for G values of 0.3, 0.3545, 0.3577, 0.3581, and 0.37.

A bifurcation diagram can be created to demonstrate this periodic doubling. This diagram shows the x-coordinate of the steady-state solution sampled at time intervals of 2π. If the solution is $2\pi n$ periodic then there will be n distinct points on the diagram.

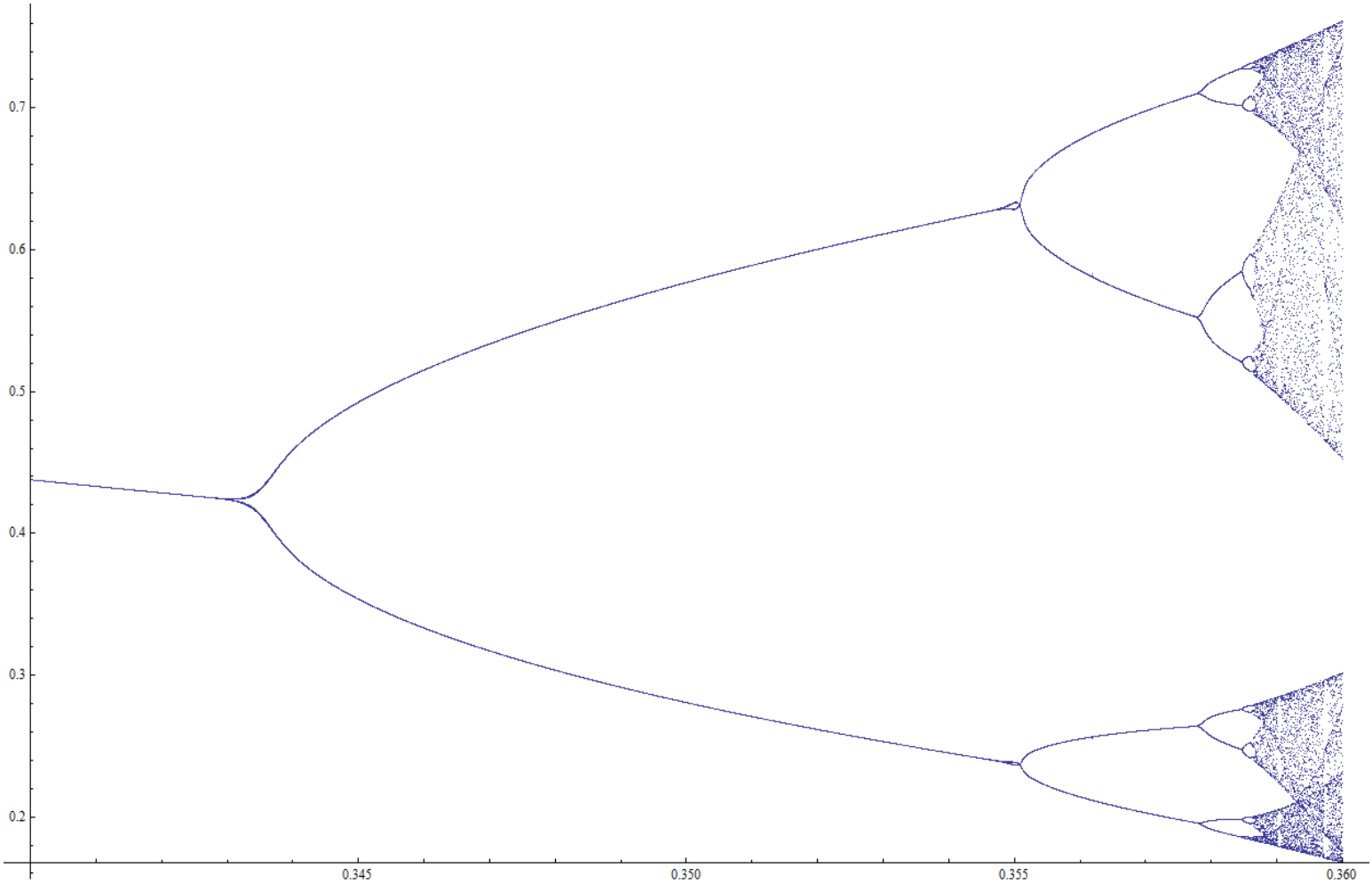

Diagram 6: Bifurcation diagram; the x-axis is the value of G and the y-axis are the x points sampled.

Diagram 6 is an example for $a = 0.5$ and $b = 1$. This was created by numerically solving the Duffing Oscillator for initial conditions $x_0 = 1,\ \dot{x}_0 = 0$ and then taking sampling the x coordinate for t values between 1000 and 1100 which are an integer multiple of 2π.

The phenomenon of period doubling can clearly be seen in *Diagram 6*. The diagram shows a clear fractal nature, as zooming in on any node of the tree will result in a diagram which looks similar to the whole diagram. At the right had side of the diagram, the number of bifurcations becomes arbitrarily large, and chaotic behaviour occurs.

By continuing to increase the driving force while keeping $a = 0.5$ and $b = 1$, further complex behaviour occurs. *Diagram 7* shows phase plot diagrams for various values of G.

Diagram 7: Limit cycles for G values (from top left to bottom right)of 0.38, 0.46, 0.52, 0.55, 0.65, and 0.83

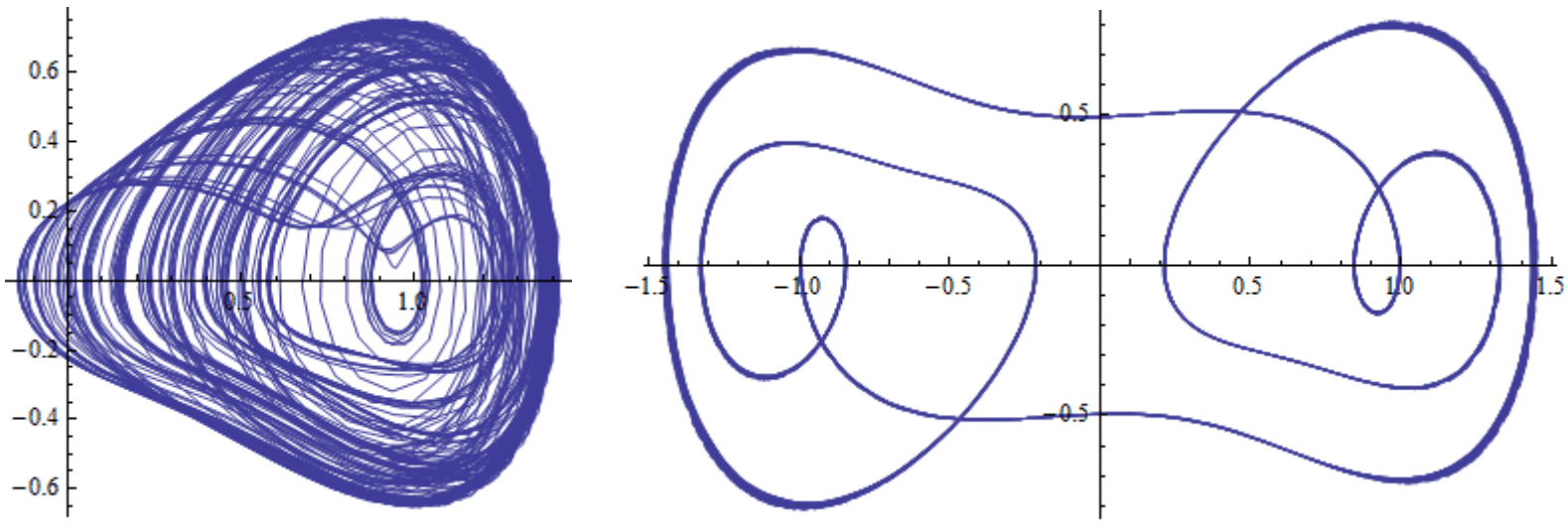

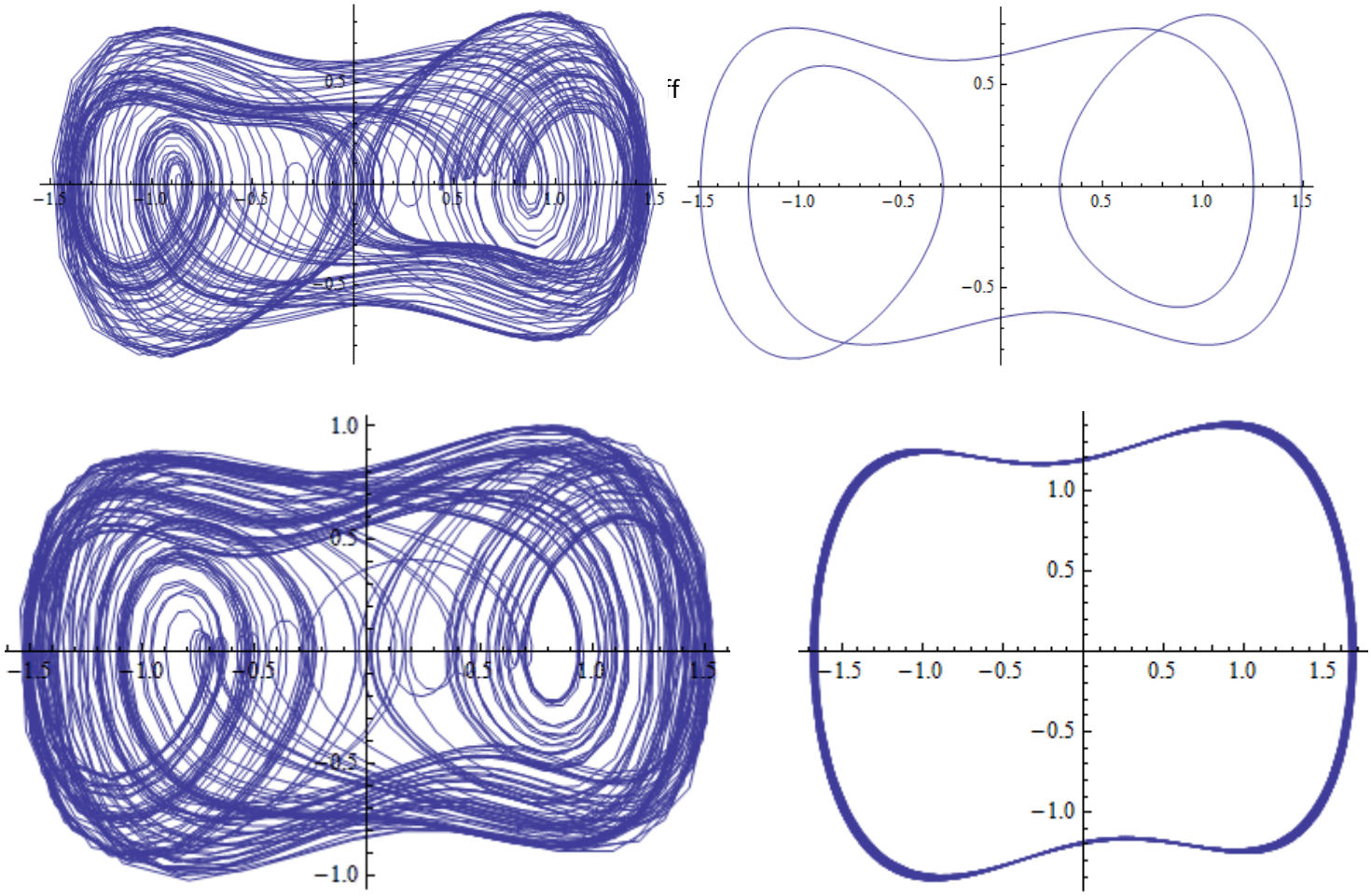

A few features should be noted. Firstly, though the Duffing Oscillator may usually be chaotic for G values between about 0.36 and 0.83, in this region there are still occasionally limit cycles. For instance at $G = 0.46$ there is a cycle of period of 10π, and at $G = 0.55$ there is a cycle of period $G = 6\pi$. Another important feature of this sequence is, for G values between 0.38 and 0.46 the Duffing Oscillator transitions from staying in one well to travelling between both. For this reason, limit cycles which occur after this transition have a symmetry of sorts upon reflection on the line $y = -x$. Finally, for G values larger than about 0.83, the Duffing Oscillator is no longer chaotic, instead forming limit cycles of period 2π similar to the one shown in *Diagram 7.* This behaviour is clearly shown in *Diagram 8*, which is a bifurcation diagram for values of G between 0.35 and 0.85.

Diagram 8: Bifurcation diagram for G between 0.35 and 0.85

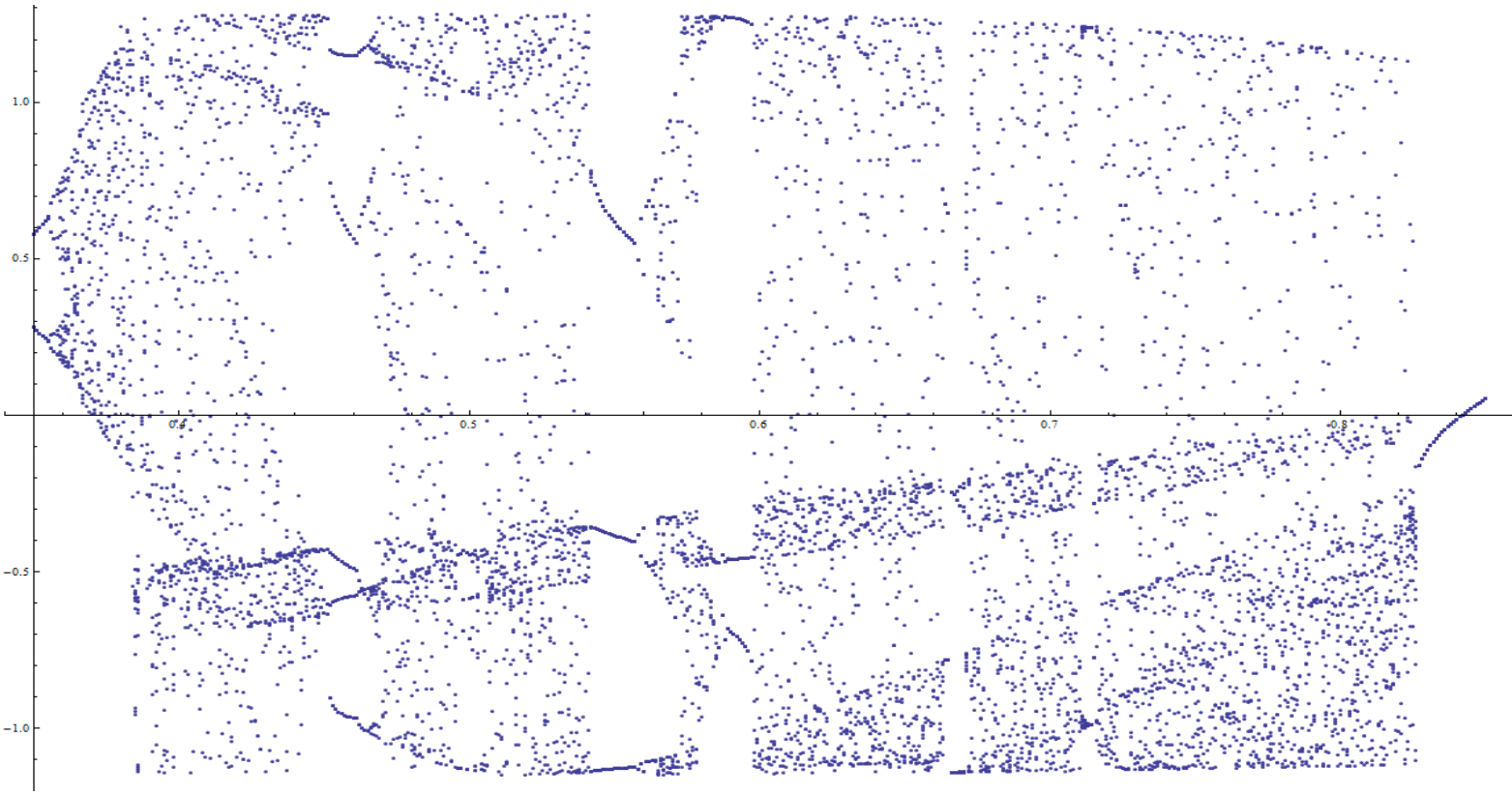

In *Diagram 8* we can see that, though the oscillator is chaotic for most values of G between 0.35 and 0.85 there are windows of periodicity, most visibly one of period 10π around $G = 0.46$ and one of period 6π around $G = 0.55$. These two regions are where the two periodic limit cycles in *Diagram 7* are found. However, these are not the only windows of periodicity, though they are the largest. For $G = 0.5$ a limit cycle of period 8π occurs, and another cycle of period 4π occurs for $G = 0.665$. A cycle of period 14π occurs when $G = 0.635$.

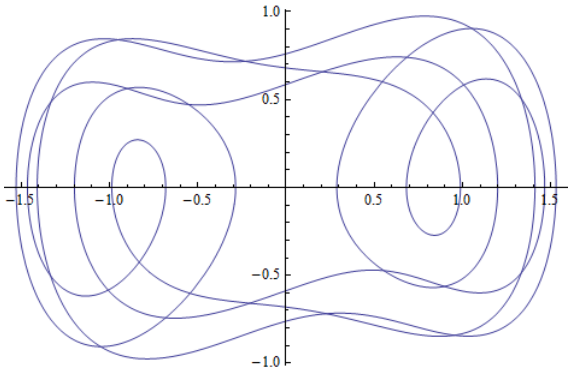

Diagram 9: A cycle of period 14π, where $G = 0.635$.

In *Diagram 10*, a bifurcation diagram is shown for the G values between 0.52 and 0.58, capturing a window of periodic behaviour. When G is between about 0.542 and 0.558 a cycle of period 6π occurs. For G values above 0.558, this gives rise to a cycle of period 12π, and then at 0.562, a period of 24π. It seems that period doubling is occurring, resulting in cycles of period $2^n 6\pi$, and this period doubling results in a return to chaotic behaviour.

The period doubling path to chaos we have just described, with the associated periodic windows, are not unique to the Duffing Oscillator. In fact, very similar behaviour can be found in the continuous systems such as the chaotic pendulum (Fitzpatrick, 2006), Chua's Diode, and the Lorentz equations, and in discrete systems such as the Henon map and the logistic map (Lakshmanan & Rajasekar, 2003). Feigenbaum demonstrated for the logistic map that r_n is the value of parameter at which a 2^n periodic cycle first appears, then:

$$F_n = \frac{r_{n-1} - r_{n-2}}{r_n - r_{n-1}}$$

Diagram 10: Bifurcation diagram for G between 0.542 and 0.558

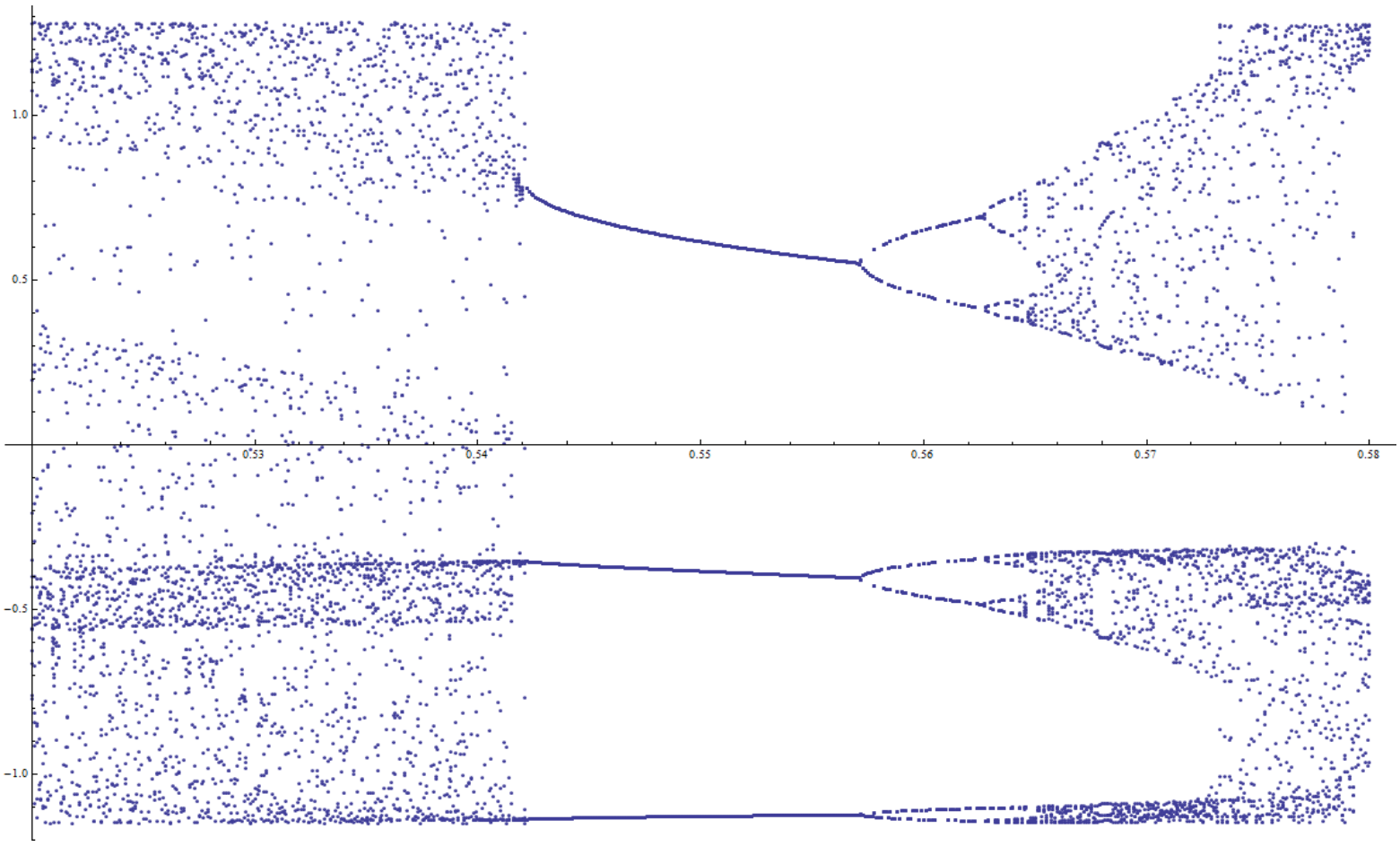

converges to a constant, $F = 4.669$, known as the *Feigenbaum ratio*. This result has been generalised to a host of discrete maps which posses a period doubling route to chaos, and has been experimentally verified in a number of different physical systems (Fitzpatrick, 2006), including the Duffing Oscillator (Jordan & Smith, 2007).

It has also been demonstrate that, for a certain class of models exhibiting a transition to chaos via period doubling, the sequence of stable periodic orbits is the same for each model, and this sequence is known as the U-sequence. For the periods up to period 6, the sequence is:

$$1, 2, 4, 6, 5, 3, 6, 5, 6, 4, 6, 5, 6.$$

It is possible to provide non-rigorous arguments to generalise this to all physical systems that have period doubling (Fitzpatrick, 2006), and in *Diagram 8* we can observe many of these cycles (though some are simply to be seen on the diagram). Thus, the behaviour we have observed for the Duffing Oscillator is not unique to the oscillator, but instead posses features which seem to be universal to a large class of mathematical models and physical systems.

3.4 Periodicity of Solutions

So far we have only explored the behaviour of the system when $a = 0.5$ and $b = 1$. We can explore the periodicity of solutions over a larger region of phase space by using a different type of plot, which I shall call periodicity plot, as shown in *Diagram 11.*

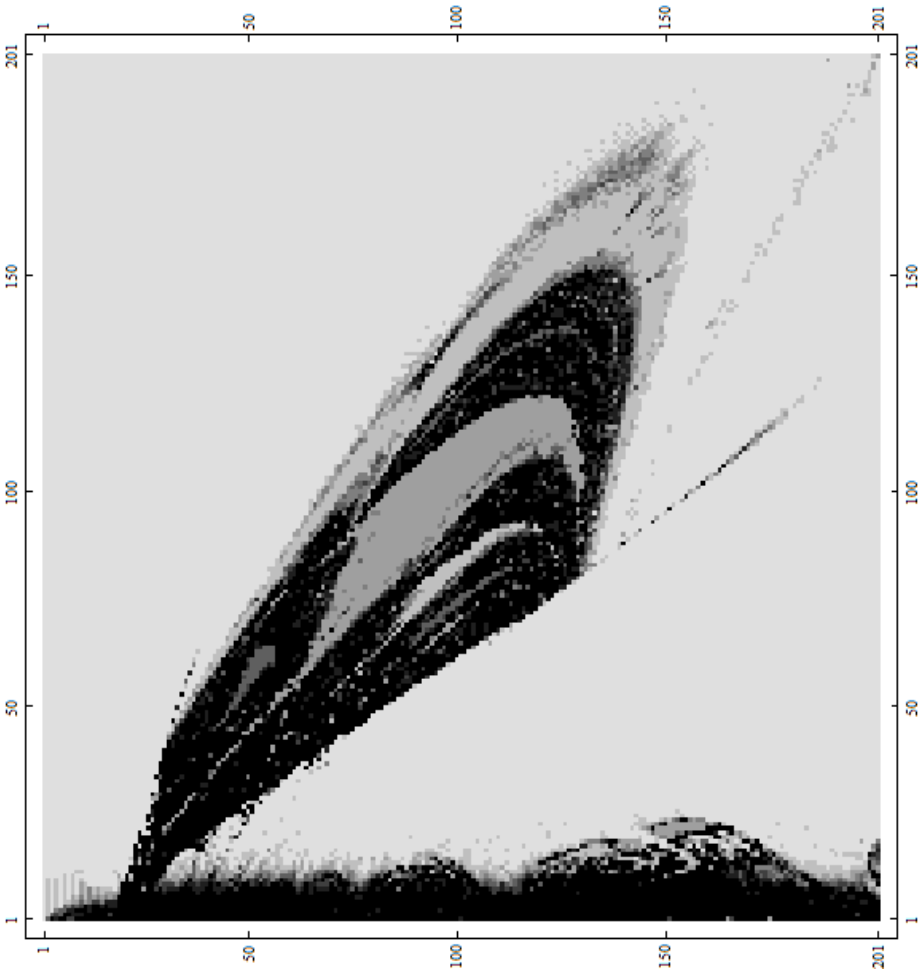

Diagram 11: Periodicity plot values of (G, a) between $(0, 0)$ and $(2, 2)$. The coordinate of a pixel can be found by subtracting one from the numbers on side and dividing by 100.

In *Diagram 11*, each pixel corresponds to a point in (G, a) space, with the darkness of the pixel corresponding the period of the limit cycle. The lightest shade of occurs when the period is 2π and the darkest shade of grey occurs when the period is larger than 12π.

The periodicity is calculated by numerically solving the Duffing Oscillator with initial conditions $x_0 = 1, \dot{x}_0 = 0$. For t values between $t = 100$ and $t = 100 + 16\pi$ which are equal to 0 in modulo 2π, the $(x, \dot{x})$ is sampled, and rounded to within 0.02. The union of the list of these values is found, and the number of elements in this list should then be the periodicity, if the periodicity is less than 16π, and should equal 16π otherwise.

This method is not perfectly accurate. The most likely error would occur in situations where the transient solution converges slowly to the limit cycle, resulting in aperiodic behaviour still being apparent in the sampling. This would result in the period of the cycle being overestimated. This is the motivation for rounding values before comparing, to prevent close values not being considered the same by the union process. However, the value to which the coordinates are rounded needs to be sufficiently small to prevent close coordinates from being considered the same, which would underestimate the periodicity of a limit cycle. Since the values are rounded to 0.02, this process should not be a problem, and we can conclude that while some values may have an overestimated periodicity, the periodicity is very unlikely to have been significantly underestimated.

Though there may be inaccuracies, *Diagram 11* still provides a good indication of the periodicity of solutions to the Duffing Oscillator. The majority of the graph shows 2π periodicity, other than for two main regions. The first is the area around the x-axis. This is the region where the damping, a is close to 0, and thus it makes sense that such solutions would not demonstrate regular periodic behaviour. There is also a roughly triangular region which does not have 2π periodicity. The chaotic region we explored earlier where $a = 0.5$ is part of this region. Along the left hand edge, the period double from 2π to 4π can be seen. It should be noted that any pixels which suggests a higher periodicity than 4π along this boundary are artefacts of the method used to produce the graph. At points near the bifurcation convergence to the limit cycle takes a longer period of time and thus for these pixels the convergence was too slow. One example of this is shown in *Diagram 12*, which plots the solution of the oscillator for $a = 1.25$, $G = 0.88$, which is shown as a black pixel on the graph. However, when we plot this for initial conditions $x_0 = 1$, $\dot{x}_0 = 0$, for values of t between 100 and 500, we can see that it does converge to a 4π limit cycle, albeit very slowly.

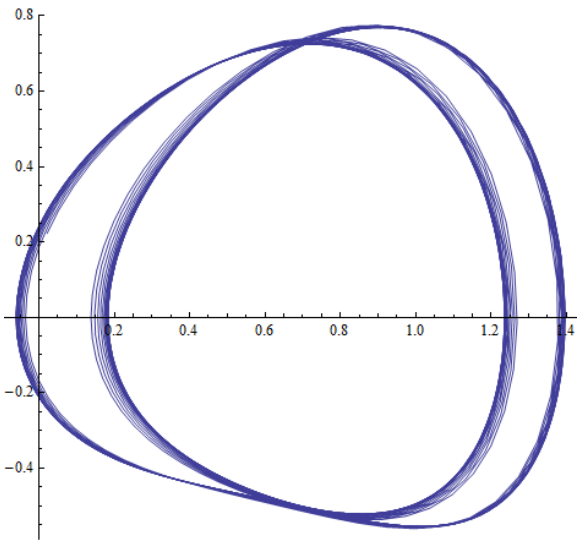

Diagram 12: Solution to the Duffing Oscillator for $a = 1.25, G = 0.88, x_0 = 1, \dot{x}_0 = 0$, where $t \in [100, 500]$.

The dark regions in the triangular region are areas where the Duffing Oscillators shows chaos. However, there are lighter regions with this area, most notably in the centre of the graph around $a = 1$ and $G = 1$. The points in this region have a periodicity of 6π, and indeed, when exploring the case of $a = 0.5$, the 6π periodic cycle we found is in this region. These light regions are periodic windows within the chaos, and we can see other regions of periodicity, for instance, around $a = 0.5$, $G = 0.5$, which has a period of 10π, and also around $a = 0.85$, $G = 1$, which has periodicity 4π.

The boundary of this chaotic region shows interesting properties. The curve at the top of the region shows clear evidence of period doubling. The two smaller boundaries are fairly straight, and don't show any evidence of period doubling. When we studied the case of $a = 0.5$, we passed through the curved boundary when G was around 0.35, and thus say period doubling. However, when we crossed from chaotic to nonchaotic behaviour when $G \approx 0.83$, we passed through one of the straight boundaries and thus did not see period halving (which is just period doubling seen from the reverse direction), but instead, the system abruptly changed from chaos into a limit cycle of period 2π.

3.5 Lyapunov Exponents

By plotting the periods of the limit cycle for various a and G values, we have been able to gather a lot of information about the system. However, this information is not enough to work out the regions in which the Duffing Oscillator shows chaos. This is because though our diagram shows the existence of non-repeating trajectories, we have so far failed to show that the system is sensitive to the initial conditions. The maximal Lyapunov exponenet provides a quantitative method of doing this (Jordan & Smith, 2007).

If a system shows sensitivity to initial conditions, then the distance between two close points in phase space should grow exponentially:

$$d(t) = d_0 e^{\lambda t}$$

The value of λ depends on the direction of the two points, allowing a value of λ to be calculated for each orthogonal direction. These values are known as the Lyapunov Characteristic exponents of the system. However, values of t become large, the growth cause by the maximum Lyapunov exponent will overwhelm the other exponents, and thus in order to determine whether a system is chaotic we only need to know the maximum Lyapunov exponent. The maximum Lyapunov exponent can thus be defined as:

$$\lambda_0 = \lim_{t\to\infty, d_0\to 0} \frac{1}{t} \ln\left(\frac{d(t)}{d_0}\right)$$

When this is positive, close points will over time separate, and combined with condition of boundedness and aperiodicity this implies that the system displays chaotic behaviour. Otherwise, the system is nonchaotic.

Calculating Lyapunov Exponents numerically is not an easy task, and a *Mathematica* package written by Marco Sandri and explained in (Sandri, 1966). *Diagram 13* shows the Lyapunov exponent calculated for values of (G, a) between $(0,0)$ and $(2,2)$ taken at 0.01 intervals. When the maximum Lyapunov exponent is less than or equal to zero the pixel is white.

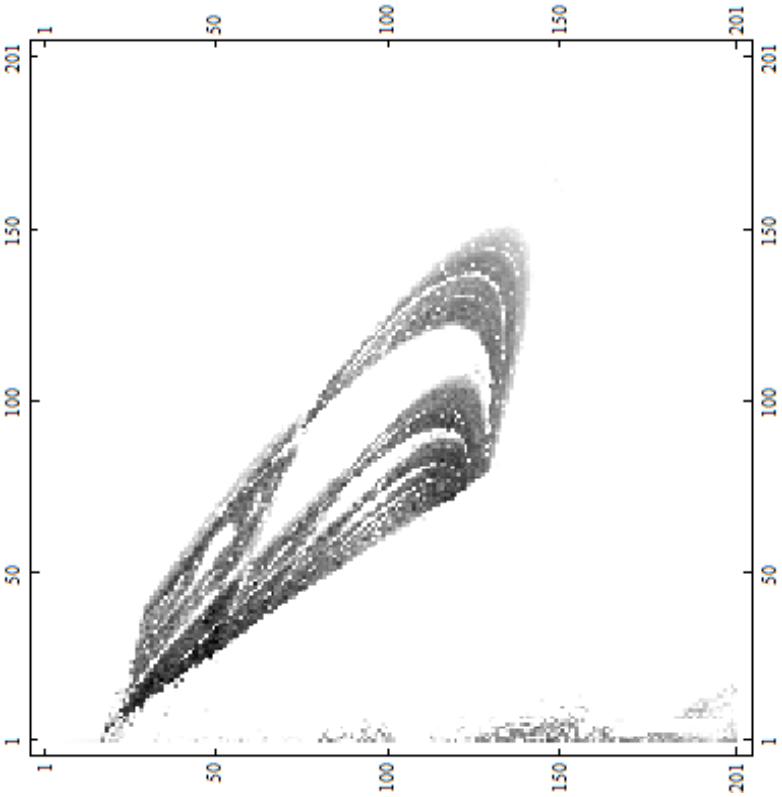

Diagram 13: Maximum Lyapunov exponent for (G, a) between $(0, 0)$ and $(2, 2)$. The coordinate of a pixel can be found by subtracting one from the numbers on side and dividing by 100.

By comparing *Diagram 11* and *Diagram 13*, we can see that the regions of positive Lyapunov exponent closely follow the regions of large periodicity in *Diagram 11*. Perhaps the most striking difference between the two is that, in *Diagram 13* the area just above the x-axis is largely non-chaotic, even though *Diagram 11* showed this region as black. This suggests that the Duffing Oscillator in this region takes a considerable amount of time to converge to the limit cycle. Periodic windows are highly visible.

4. Poincare Section

4.1 Fractal Nature of the Poincare Section

It is difficult to study the structure of chaotic solutions to the Duffing Oscillator by plotting trajectories in phase space. For instance, the chaotic plots shown in *Diagram 7* are not easy to interpret because of the complexity of the orbit. In order to study chaotic trajectories, another tool, called the Poincare section, is often useful (Lakshmanan & Rajasekar, 2003).

A Poincare section can be created by sampling the value of $\big(x(t), \dot{x}(t)\big)$ at time intervals of 2π and then plotting these in phase space. An example of such a plot for $a = 0.2$, $G = 0.3$, $b = 1$ is shown in *Diagram 14*. This was generated with initial conditions $x_0 = 1$, $\dot{x}_0 = 0$, and the Poincare section was generated for t values between 100 and $2\,000\,000$, with the condition that $t \equiv 0 \pmod{2\pi}$.

The structure of this section is quite complicated, as can be seen in the diagram. It is not, however, random; though the Duffing Oscillator is chaotic in this region, the Poincare section still shows an intricate structure.

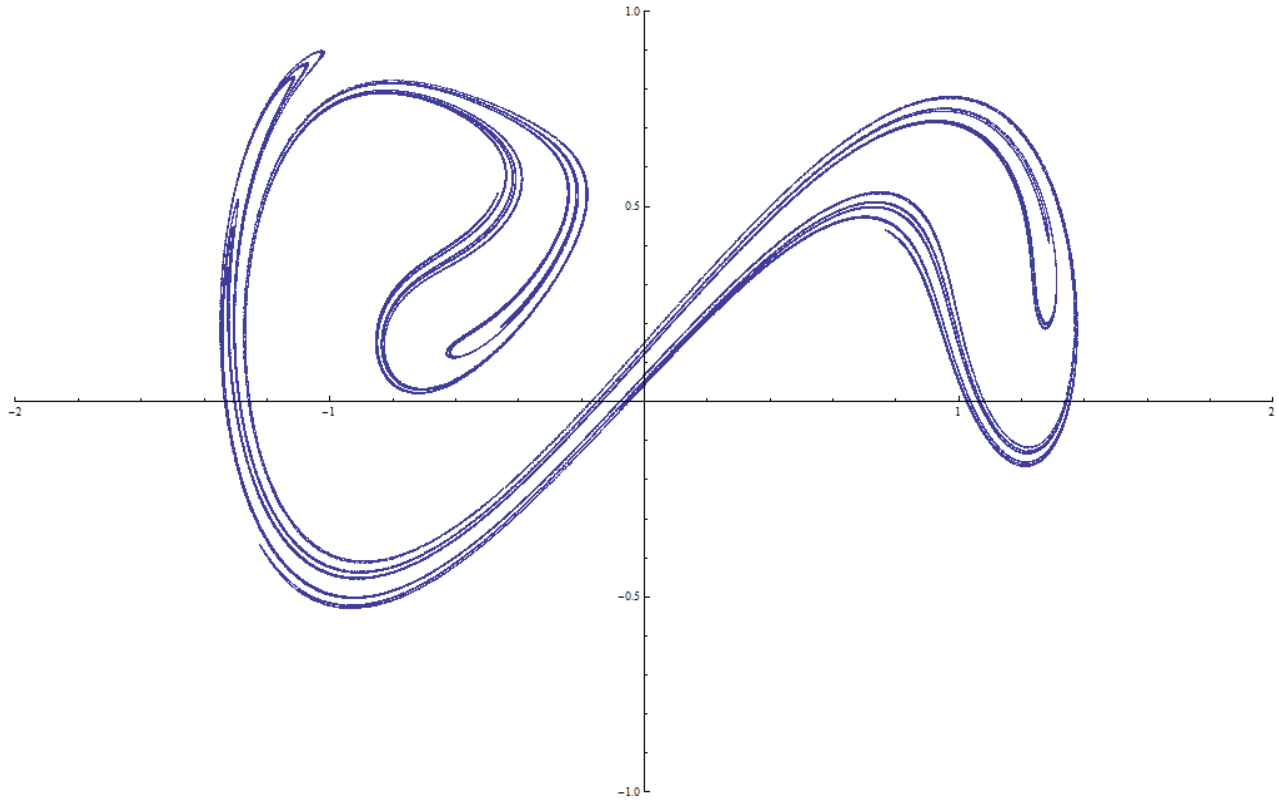

Diagram 14: Poincare Section for a=0.2, G=0.3. Two million points are shown.

There are many definitions of what it means for a set to be a fractal. Perhaps the two most important features of fractals are self-similarity and non-integer fractal dimensions (Falconer, 1990). We shall now show that the Poincare section has both, and can therefore be considered to have a fractal nature. By zooming in at various locations, we can see evidence of self-similarity, as shown in

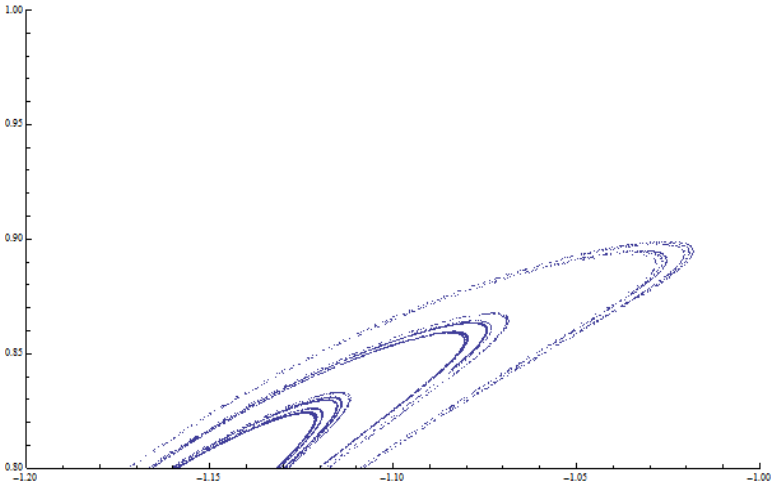

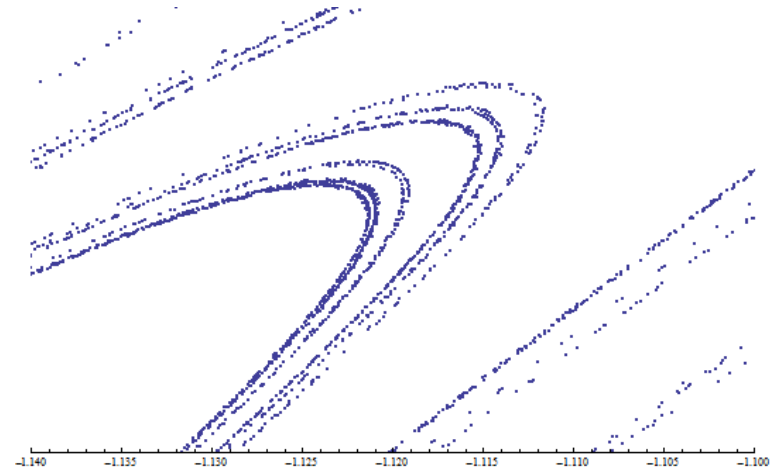

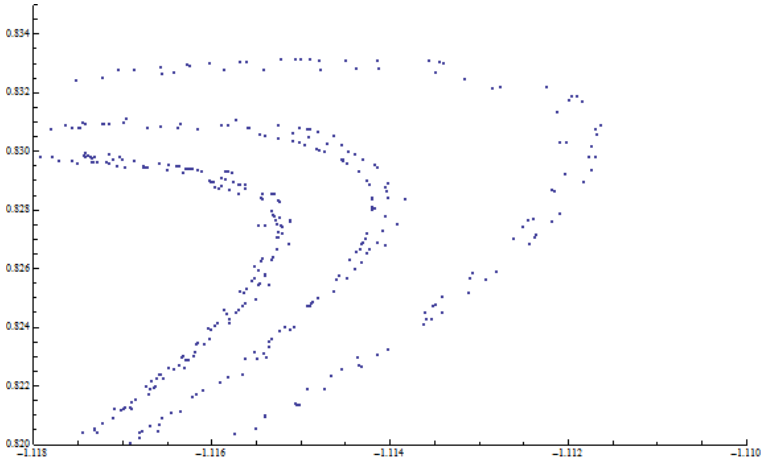

Diagram 15: Poincare section for a=0.2, G=0.3, zoomed in on the rectangle with vertices (-1.2, 0.8), (-1, 1) (left), (-1.14, 0.8) , (-1.1, 0.84) (bottom right), and (-1.118, 0.820), (-1.1, 0.835) (bottom left)

Diagram 15. This type of self-similarity is known as self-similarity is known as quasi self-similarity, as whilst the same pattern emerges at different length scales, the pattern is not repeated exactly but rather distorted. The existence of self-similarity results in complex patterns occurring on every length scale of the fraction, a common feature shared by all fractal.

Another crucial feature of a fractal is having a non-integer fractal dimension. Perhaps the simplest such dimension is given by the box-counting dimension (Falconer, 1990). This is most commonly defined as:

$$\dim_{box}(S) = \lim_{\varepsilon \to 0} \frac{\log\big(N(\varepsilon)\big)}{\log(\varepsilon^{-1})}$$

where ε is the length of the side of a box, and $N(\varepsilon)$ is the number of such boxes required to cover the set S. However, for numerical purposes it is more convenient to use the mesh definition, which divides up the space into a grid of squares of length ε. The number $N(\varepsilon)$ is then defined as the number of squares containing a subset of S, and the formula:

$$\dim_{box}(S) = \lim_{\varepsilon \to 0} \frac{\log\big(N(\varepsilon)\big)}{\log(\varepsilon^{-1})}$$

then yields the same value as the box-counting method (Falconer, 1990). By letting $\varepsilon = 2^n$, and taking the logarithm to be in base 2, we can write:

$$\dim_{box}(S) = \lim_{n \to \infty} \frac{\log_2\big(N(2^{-n})\big)}{n}$$

Taking S to be the Poincare section for t values between 100 and 20 000 000, we can calculate $\log_2\big(N(2^{-n})\big)$ and plot this against n. The gradient of this line will then provide a good approximation of the fractal dimension. This is shown in *Diagram 16*. As can be seen from the graph, the line of best fit provides a very good approximation of $N(2^{-n})$, with an R^2 value of 0.9995. The

Diagram 16: Number of Boxes vs Length of Boxes

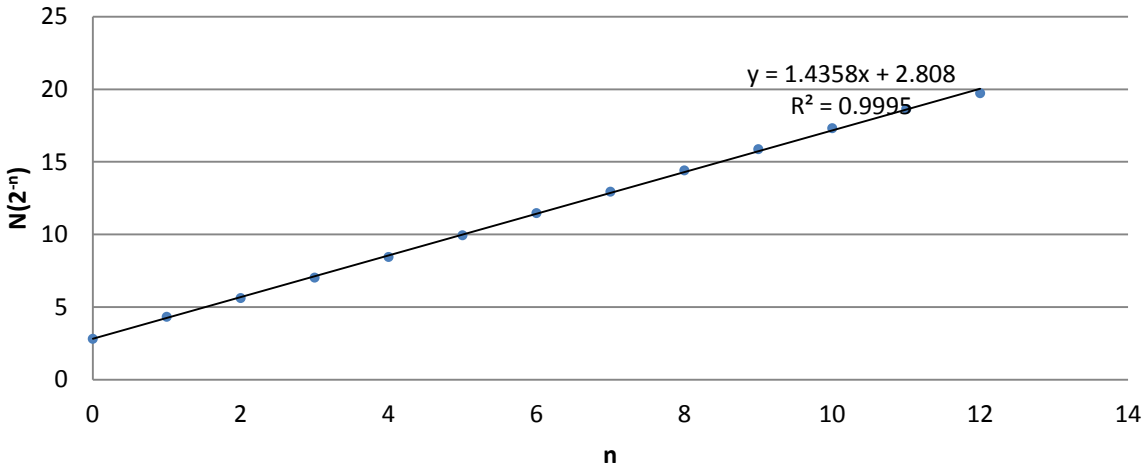

gradient of the line of best fit is 1.4358, and therefore the box-counting dimension of the Poincare section is about 1.44. We can conclude that the Poincare section has a non-integer fractal dimension, another feature of fractals.

4.2 Evolution of a Poincare Section

The Poincare section we just studied was comprised of $\big(x(t), \dot{x}(t)\big)$ points for $t \equiv 0 \pmod{2\pi}$. We can witness the evolution of the Poincare section over a 2π time period by plotting Poincare sections where $t \equiv \tau \pmod{2\pi}$ where $\tau \in [0,2\pi]$. *Diagram 17* shows the Poincare section for values of τ that are integer multiples $\frac{\pi}{4}$. In each Poincare section 100 000 points have be plotted.

Diagram 17: Poincare section for $\tau = \frac{n\pi}{4}$, where, from top left to bottom right, $n = 0, 1, 2 \dots 7$.

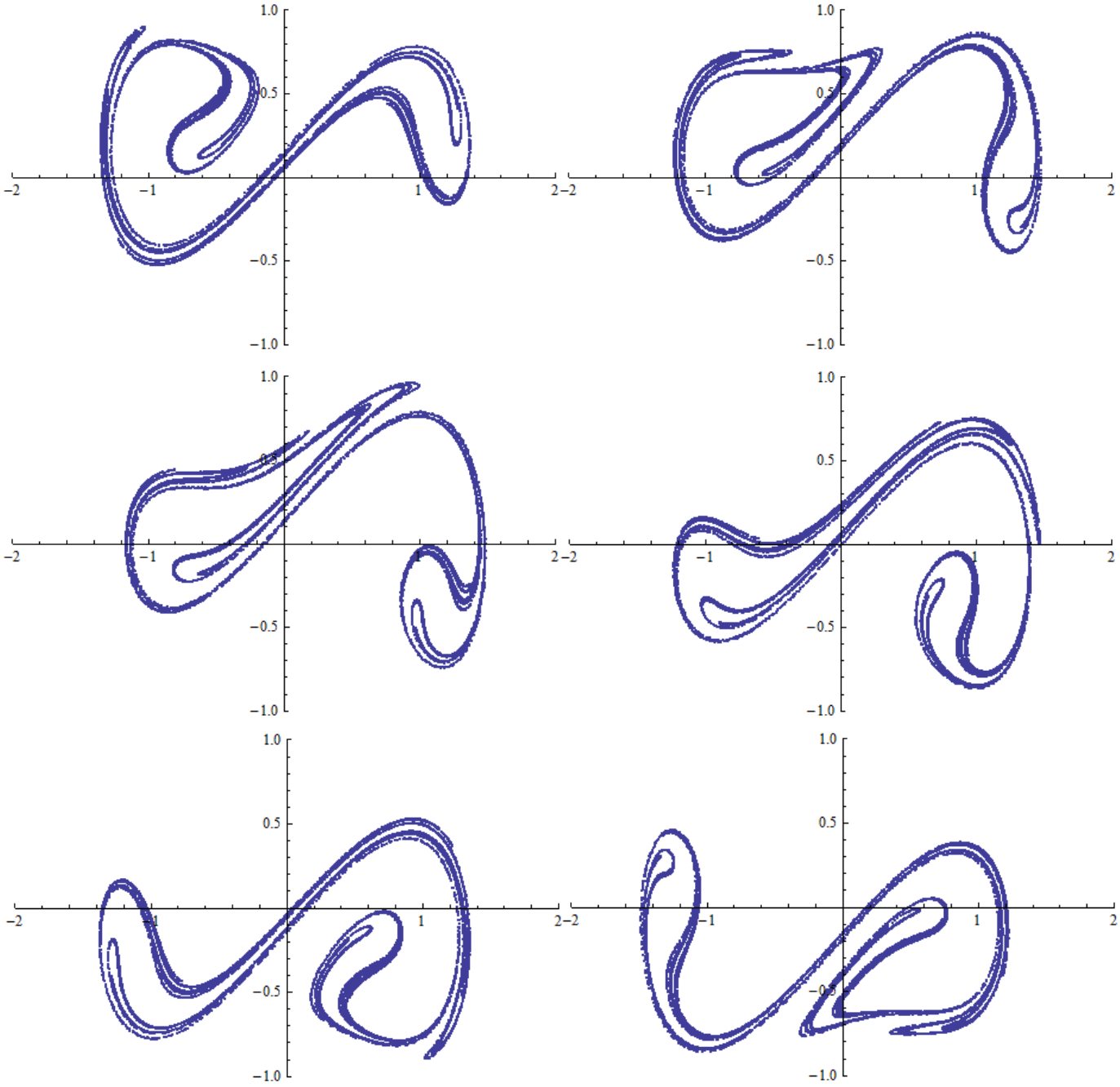

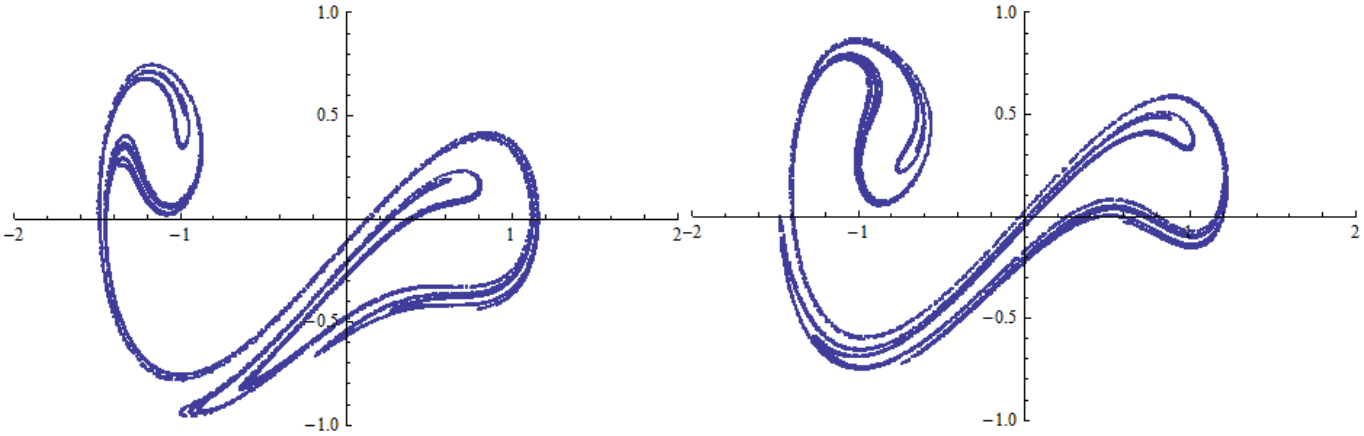

The last plot in *Diagram 17* can leads directly back into the first plot, as if $\tau = 2\pi$ then this equavalent to $\tau = 0$. For this reason *Diagram 17* can be seen as a loop. One interesting feature of *Diagram 17* is that each plot is very similar to the plot four along, that is, to the plot where the τ value differes by π. This can most clearly be seen by rotating one plot 180 degrees.

The reason for this probably originates because of a symmetry of the Duffing Oscillator. It has been shown that if $x(t)$ is a solution to the Duffing Oscillator, then so is $(-1)x(t + \pi)$. In the phase plane this corresponds to the moving π units of time forward and rotating the phase plane 180 degrees, which is exactly the relationship between each two similar plots. However, it must be noted that the plots are not exactly the same, as due to symmetry this can only occur in a 2π cycle.

Diagram 17 can be used to explain the occurrence of self-similarity in the Poincare Section. Take a part of the Poincare section; say one of the large curves. As time marches forward the loop is distorted, but there is no evidence of discontinuity in the process. Instead, the loop is folded into itself, and after a full period of driving this results in the loop has remained topologically intact, but part of it now has been stretched to form a new loop identical to the original, and part of it now forms a smaller loop within the first loop. This process can be extrapolated to occurring for any structure within the Poincare section, resulting in smaller and more intricate structures present at every length scale. As the Poincare section is the same as the Poincare section after 2π units of time have passed, this process of stretching and folding can explaining the fractal nature of the Poincare Section.

5. Conclusion

The behaviour of Duffing Oscillator was explored throughout the paper in both chaotic and non-chaotic regimes. After first discussing the physical significance of the Oscillator, the Duffing equation was reduced to a dimensionless form. This equation was then solved in three different approximations, demonstrating the existence of limit cycles in certain regimes. The chaotic nature of certain regions of the parameter space was then developed, both through a qualitative study of a particular case in order to show period doubling, and also through quantitative studies of periodicity and Lyapunov exponents. A Poincare section from the chaotic region of the oscillator was studied, and the fractal nature of this diagram was explained both qualitatively and through the calculation of a fractal dimension.

6. Bibliography

Falconer, K. (1990). *Fractal Geometry: Mathematical Foundations and Applications.* Chichester: John Wiley & Sons.

Fitzpatrick, R. (2006, 03 29). *The chaotic pendulum*. Retrieved 03 21, 2014, from Richard Fitzpatrick: http://farside.ph.utexas.edu/teaching/329/lectures/node46.html

Jordan, D. W., & Smith, P. (2007). *Nonlinear Ordinary Differential Equations.* New York: Oxford University Press.

Kanamaru, T. (2008). *Duffing Oscillator*. Retrieved 03 22, 2014, from Scholarpedia: http://www.scholarpedia.org/article/Duffing_oscillator

Kaplan, D., & Glass, L. (1995). *Understanding Nonlinear Dynamics.* New York: Springer-Verlag.

Lakshmanan, M., & Rajasekar, S. (2003). *Nonlinear Dynamics.* New York: Springer-Verlag.

Sandri, M. (1966). Numerical Calculations of Lyapunov Exponents. *The Mathematica Journal* , 78-84.

Tamasevicuite, E., Tamasevicius, A., Mykolaitis, G., Bumeliene, S., & Lindberg, E. (2008). Analogue Electrical Circuit for Simulation of the Duffing-Holmes Equation. *Nonlinear Analysis: Modelling and Control* , 241-252.